Toward reversing Joule heating with a phonon-absorbing heterobarrier

Seungha Shin*
Department of Mechanical, Aerospace and Biomedical Engineering, University of Tennessee, Knoxville, Tennessee 37996, USA

Massoud Kaviany
Department of Mechanical Engineering, University of Michigan, Ann Arbor, Michigan 48109, USA
(Received 12 March 2014; revised manuscript received 10 December 2014; published 2 February 2015)

Using a graded heterobarrier placed along an electron channel, phonons emitted in Joule heating are recycled *in situ* by increasing the entropy of phonon-absorbing electrons. The asymmetric electric potential distribution created by alloy grading separates the phonon absorption and emission regions, and emission in the larger effective-mass region causes momentum relaxation with smaller electron kinetic energy loss. These lead to smaller overall phonon emission and simultaneous potential-gain and self-cooling effects. Larger potential is gained with lower current and higher optical-phonon temperature. The self-consistent Monte Carlo simulations complying with the lateral momentum conservation combined with the entropy analysis are applied to a GaAs:Al electron channel with a graded heterobarrier, and under ideal lateral thermal isolation from surroundings, the phonon recycling efficiency reaches 25% of the reversible limit at 350 K, and it increases with temperature. The lateral momentum contributes to the transmission across the barrier, so partially nonconserving lateral momentum electron scattering (rough interface) can improve efficiency.

DOI: 10.1103/PhysRevB.91.085301 PACS number(s): 63.20.kd, 73.40.Kp, 74.25.Kc, 79.60.Jv

I. INTRODUCTION

In circuits, the electric potential is converted to a phonon in Joule heating and the system entropy increases, while maintaining electron momentum, under an otherwise accelerating electric field. Before their equilibration and further increase in entropy, there is an opportunity to recycle these emitted phonons, i.e., partially reverse the Joule heating. An analogous idea was suggested for radiation-balanced lasers by recycling the emitted phonons (nonradiative decay) through the anti-Stokes fluorescence [1,2]. In semiconductors, the drifting electrons (e) interact with phonons (p), converting energy, with the kinetics controlled by the electron kinetic energy ($E_{e,k}$) and the phonon occupancy (f_p) with the energy and momentum conservation constraints [3,4]. The optical-phonon interactions dominate in semiconductors, and the low-energy electrons, especially those with energy lower than the optical-phonon energy ($E_{p,O}$), have a higher absorption rate compared to emission, so a larger population of those electrons is desired for favorable phonon absorption. This nonequilibrium population distribution can be created behind a potential barrier.

Using the band discontinuity formed by alloying (e.g., GaAs/GaAs:Al), we have designed the heterobarrier structure in Figs. 1(a)–1(d) [5,6], which is aimed at returning the emitted phonons to the electric potential. The doping density is uniform and moderate ($<10^{23}$ m^{-3}, assuming nondegenerate electrons), so the equilibrium electron density is also uniform and the e-p interactions dominate. For a barrier followed by a forward field, the Al content abruptly increases and gradually decreases [Fig. 1(a)], and the electric potential [Fig. 1(b)] has a similar distribution except for the uniform background electric field ($e_{e,\mathrm{bg}}$). Electrons in the accelerating e-field relax by emitting optical phonons, which in turn can downconvert to acoustic phonons, and due to the larger phonon emission rate compared to the downconversion rate of the emitted phonons, the optical phonons are overpopulated without a barrier [although the overpopulation is not significant except for a large e-field ($>10^6$ V/m)] [7]. Differing from phonon emission under a uniform e-field, the heterobarrier structure creates a phonon-absorption-favorable condition. The large phonon absorption leads to upconversion of the acoustic phonons [Fig. 1(c)] [8], so the barrier structure harvests acoustic phonons in addition to the optical phonons. As the emitted phonons are reabsorbed in the barrier transition, reducing the potential loss (equivalent to Joule heating) in electric current, the barrier structure recycles the emitted phonons [Fig. 1(d)]. The emitted phonons can also leave the channel to the surroundings, however under ideal lateral thermal isolation assumed here, the only other phonon outlet is through the channel ends.

Here, we introduce a method (based on electron-barrier–transition architecture and conditions) for creating nonequilibrium occupancy in favor of net phonon absorption, i.e., reduced net emission of the phonons along the electron drift path. Using the self-consistent Monte Carlo (MC) simulations complying with the lateral momentum conservation combined with the entropy analysis, we optimize the phonon-absorption region within the electron channel with the graded heterobarrier structure. The thermionic cooling achieved by the optical-phonon absorption is similar to that treated in [9], but here the phonon emissions up- and downstream of the graded barrier are included, so the recycling of the emitted phonons is aimed at partially reversing the Joule heating.

II. GRADED BARRIER: NONEQUILIBRIUM CONDITION FOR PHONON ABSORPTION

The electron energy and momentum distributions are altered by the electric field through the governing equations [3]

$$\mathbf{u}_e = \frac{d\mathbf{r}_e}{dt} = \frac{1}{\hbar}\nabla_{\boldsymbol{\kappa}_e} E_{e,k} \quad \text{and} \quad \frac{d\boldsymbol{\kappa}_e}{dt} = \frac{e_c \mathbf{e}_e}{\hbar}, \tag{1}$$

*sshin@utk.edu

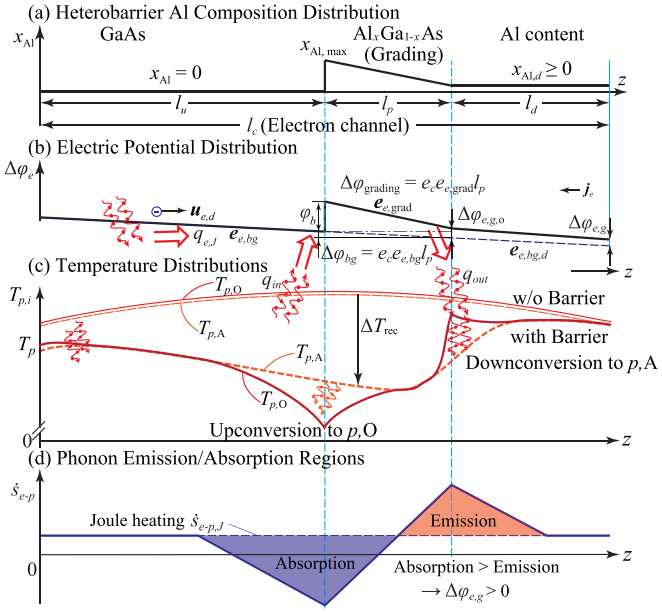

FIG. 1. (Color online) Schematic of the phonon recycling using the graded heterobarrier structure in an electron channel. (a) Al content (x_{Al}), and (b) the electric potential distributions throughout the heterobarrier structure. (c) Variations of the temperature and (d) phonon emission rate along the channel and comparison with a channel with no barrier. The potential distribution is created by the band discontinuity controlled by the x_{Al} variation, and this structure induces the local phonon absorption/emission-favorable regions. Since the interaction with the optical phonons has the highest probability, the optical-phonon population varies with the interaction kinetics, but the up- and downconversion by the three-phonon interaction processes quickly recover from the nonequilibrium created between the optical- and acoustic-phonon temperatures ($T_{p,O}$ and $T_{p,A}$) [5]. The absorption and emission rates are made relative to the uniform Joule heating, and with larger absorption compared to emission there is an electron potential gain ($\Delta\varphi_{e,g}$).

where $\mathbf{r}_e$ and $\mathbf{u}_e$ are electron position and velocity vectors, $\hbar$ is the reduced Planck constant, $\boldsymbol{\kappa}_e$ is the electron wave vector, $\mathbf{e}_e$ is the electric-field vector, and e_c is the electron charge. The one-dimensional (1D) electron channel with ideal lateral thermal isolation from the surroundings is shown in Fig. 2(a). The lateral momentum is conserved in the absence of scatterings [10,11], and along with the parabolic band structure and the energy conservation, the z-direction wave vector after the potential change $\Delta\varphi_e$ (subscripts 1 and 2 refer to the states before and after the barrier transition) is

$$\kappa_{e,z,2}^2 = \kappa_{e,z,1}^2 - \frac{2m_{e,e}\Delta\varphi_e}{\hbar^2}. \tag{2}$$

This is derived from Eq. (1) using $e_{e,z} = -\Delta\varphi_e/e_c l$. The potential barrier φ_b is equal to $\Delta\varphi_e$ in the limit of $l \to 0$ with infinitely large field $-(\varphi_b/e_c)\delta(z)$, where $\delta(z)$ is the delta function. However, in electron scattering by the barrier, the lateral momentum can change during the barrier transition, depending on the interface condition. Fully nonconserving lateral momentum (over the entire electron wavelength spectrum) has been applied to rough barrier interfaces [5,12] and represents one of the limits. The other limit is the fully conserving lateral momentum (ideally smooth interface), which is the most restrictive and is used here to assess the phonon recycling under such a condition.

The local potential distribution can be controlled by an external potential, such as the gate voltage [13,14], which requires additional structure, but here we employ the band discontinuity of the heterojunction [15,16]. The band-gap discontinuity is controlled by alloying (here Al composition), and in particular the discontinuity in the conduction band ($\Delta E_{e,c}$) is the potential barrier with height φ_b for the electrons. For example, $\Delta E_{e,c} = 0.79 x_{Al}$ eV at the interface of Al$_x$Ga$_{1-x}$As/GaAs [17,18], where x_{Al} is the Al atomic fraction. This also causes the effective mass $m_{e,e}$ alteration, i.e., $m_{e,e}/m_{e,o} = 0.063 + 0.083 x_{Al}$ in the Al$_x$Ga$_{1-x}$As system, where $m_{e,o}$ is the free-electron mass [19].

Including the effective-mass change $\Delta m_{e,e} (= m_{e,e,2} - m_{e,e,1})$ across the heterobarrier φ_b, Eq. (2) becomes

$$\kappa_{e,z,2}^2 = \kappa_{e,z,1}^2 - \frac{2m_{e,e,2}\varphi_b - 2\Delta m_{e,e} E_{e,k,1}}{\hbar^2}, \tag{3}$$

with the constraint for the barrier transition,

$$\kappa_{e,z,2}^2 = \frac{m_{e,e,2}}{m_{e,e,1}}\left(\frac{\Delta m_{e,e}}{m_{e,e,2}}\kappa_{e,x,1}^2 + \frac{\Delta m_{e,e}}{m_{e,e,2}}\kappa_{e,y,1}^2 + \kappa_{e,z,1}^2 - \frac{2m_{e,e,1}\varphi_b}{\hbar^2}\right) > 0. \tag{4}$$

With the $m_{e,e}$ increasing with the potential, the transmitted $\kappa_{e,z,1}$ should be larger than the oblate ellipsoid surface B in Fig. 2(b). The length of the lateral direction, the semiprincipal axes in the ellipsoid, is $(m_{e,e,2}/\Delta m_{e,e})^{0.5}$ times longer than the z-direction length $\kappa_{e,b}$ $[=(2m_{e,e}\varphi_b)^{0.5}/\hbar]$. On the other hand, for $m_{e,e,1} > m_{e,e,2}$, the transmission threshold appears as the hyperboloid surface C in Fig. 2(b). With larger mass on barrier ($m_{e,e,1} < m_{e,e,2}$), more electrons are transmitted through the barrier, and the wave-vector change $\Delta\kappa_{e,z}$ due to the barrier transition depends on the lateral momentum $\kappa_{e,x\text{-}y}$ $[=(\kappa_{e,x}^2 + \kappa_{e,y}^2)^{0.5}]$ as well as the transport direction $\kappa_{e,z}$ (larger $\kappa_{e,z}$ or $\kappa_{e,x\text{-}y}$, smaller $\Delta\kappa_{e,z}$).

Without scattering, the electron momentum depends only on the potential. Since a potential increase leads to momentum loss, to avoid the current loss (for momentum recovery), a higher forward field or potential drop should follow the potential increase. The phonon recycling using the barrier results in reduced phonon emission (thus potential gain) compared with no barrier present, and the potential gain exists when the net potential drop is smaller than that without the barrier, under the same current.

When an asymmetric potential distribution, including a barrier at z_o and a forward field between z_o and $z_o + l_p$, is located between two reservoirs (L and R), as in Fig. 2(c), the e distributions in $\boldsymbol{\kappa}_e$ space can be directly calculated assuming the ballistic transport (without scattering). The electrons moving in the $z(+)$ direction are reflected when the constraint for $\kappa_{e,z}$ in Eq. (4) is not satisfied. The transmitted electron momentum is calculated by Eq. (3), and the electrons gain momentum as they are accelerated by the high field after the barrier transition. If the electrons from reservoir R do not have enough momentum to overcome the barrier, they will be reflected not at a single point but on the graded barrier region

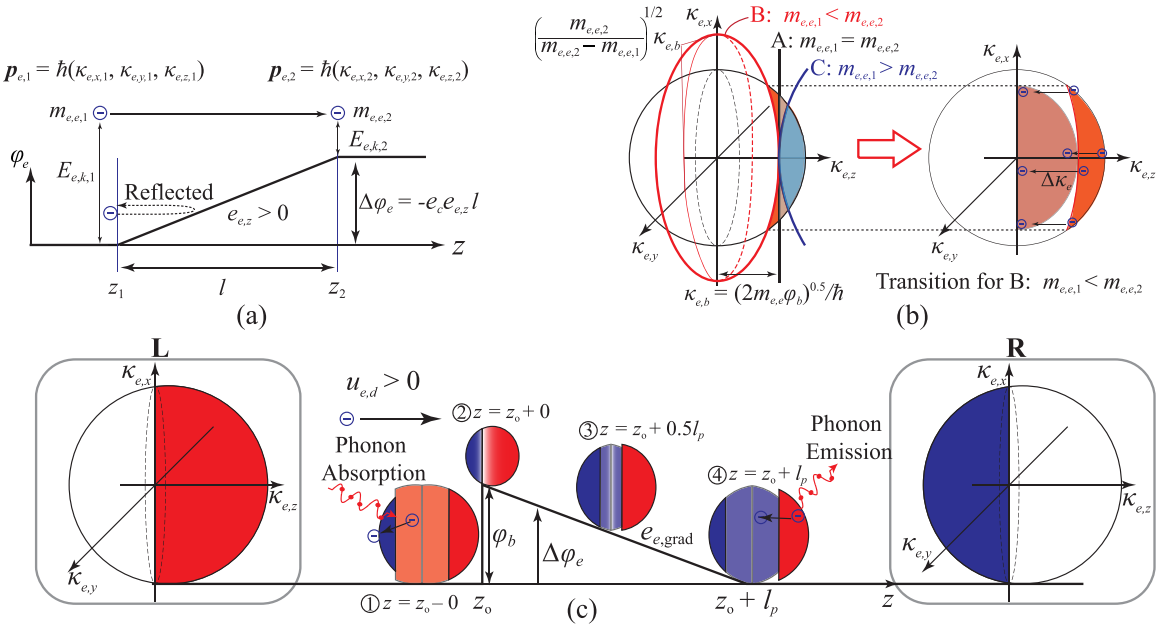

FIG. 2. (Color online) (a) The electron energy and momentum both change with the z-direction electric field (0, 0, $e_{e,z}$) applied between z_1 and z_2. (b) The electron wave-vector transition by the potential barrier or the electric field ($\varphi_b = -e_c e_{e,z} l$). While the barrier transmission with constant $m_{e,e}$ is divided by the planar surface A in $\boldsymbol{\kappa}_e$ space, the electrons with $\kappa_{e,z}$ larger than the ellipsoid B can cross the barrier for $m_{e,e,1} < m_{e,e,2}$ and the hyperboloid C marks the region for $m_{e,e,1} > m_{e,e,2}$. The change $\Delta\kappa_{e,z}$ also depends on the lateral momentum. (c) The electron distribution along with the barrier structure with the electron flowing from reservoir L to reservoir R. Dark color (red and blue) is for the transmitted electrons, and light color is for the reflected electrons.

after moving up to the point corresponding to their $\kappa_{e,z}$. With reflection, they are located in the positive $\kappa_{e,z}$ domain (forward direction velocity) in $\boldsymbol{\kappa}_e$ space. With an isotropic, initial e distribution (no drift velocity $u_{e,d}$), the electron population changes with the potential distribution (smaller population on the barrier), maintaining zero net drift velocity (symmetric e distribution throughout the channel).

Under electric current, the two reservoirs initially have the skewed distributions in the same direction, but with different potentials. When considering an e distribution shifted to the $\kappa_{e,z}(+)$ direction with nondegeneracy, the shift in the e distribution is proportional to the electric current, and the width of the distribution increases with temperature. With a drift, the e distribution is no longer in equilibrium favoring the phonon emission (Joule heating), and under a uniform field, the phonon emission increases with a more pronounced e-distribution asymmetry under larger current.

The asymmetric e distribution under current leads to a larger population of the reflected electrons before the barrier [position 1 in Fig. 2(c)] compared to that in the reservoirs (within the same range of $\kappa_{e,z}$), and this can produce extra phonon absorption. Since the change in the electron momentum by the potential height is reduced as the initial momentum increases [according to Eqs. (2) and (3)], the population and momentum in the negative $\kappa_{e,z}$ domain decrease more than that in the positive domain (as the potential increases). Thus, the electrons on the barrier $[z_o, z_o + l_p]$ have larger average velocity and phonon emission rate (due to a larger decrease in the phonon-absorbing compared to the phonon-emitting electron population). Also, downstream of the barrier [position 4 in Fig. 2(c)], the electrons with low $\kappa_{e,z}$ and $E_{e,k}$ are underpopulated, thus increasing the net phonon emission (reducing absorption). If the electrons flow from R to L or the e distribution is shifted to the $\kappa_{e,z}(-)$ direction, the absorption-favorable condition is created in that part of the barrier.

The net phonon absorption $\dot{s}_{p\text{-}e}$ ($=-\dot{s}_{e\text{-}p}$, negative net phonon emission) is calculated by the integration of the net absorption rate over the energy range, and $\dot{s}_{p\text{-}e}$ upstream of the barrier [$z = z_o - 0$, position 1 in Fig. 2(c)] depends on the relative population of absorption-favorable electrons compared to emission-favorable ones among the reflected electrons. As shown in Fig. 3(a) (considering dominance of polar optical phonon interactions), $\dot{s}_{p\text{-}e}$ at $z = z_o - 0$ first increases but then decreases at high drift velocity (current). Due to the heavy effective mass downstream of the barrier and larger interaction rates (i.e., higher Al content), the barrier region is more resistive to the electron transport. So, a long graded barrier length hinders current maintenance, and this length should be kept close to the mean free path (~60 nm) [5].

A high barrier height results in a larger effective-mass difference, but it also results in a larger resistance. With smaller barriers (φ_b), reflection of the absorption-favorable electrons is more significant compared to the emission-favorable ones, but as φ_b or drift velocity (current) increases, more emission-favorable electrons are reflected, and this reduces the net phonon absorption before the barrier. So the $\dot{s}_{p\text{-}e}$ at position 1 in Fig. 2(c) (before the barrier) begins to decrease with φ_b after reaching a maximum, as shown in Fig. 3(b), and the barrier height resulting in the maximum $\dot{s}_{p\text{-}e}$ decreases with the drift velocity (more pronounced asymmetric e distribution).

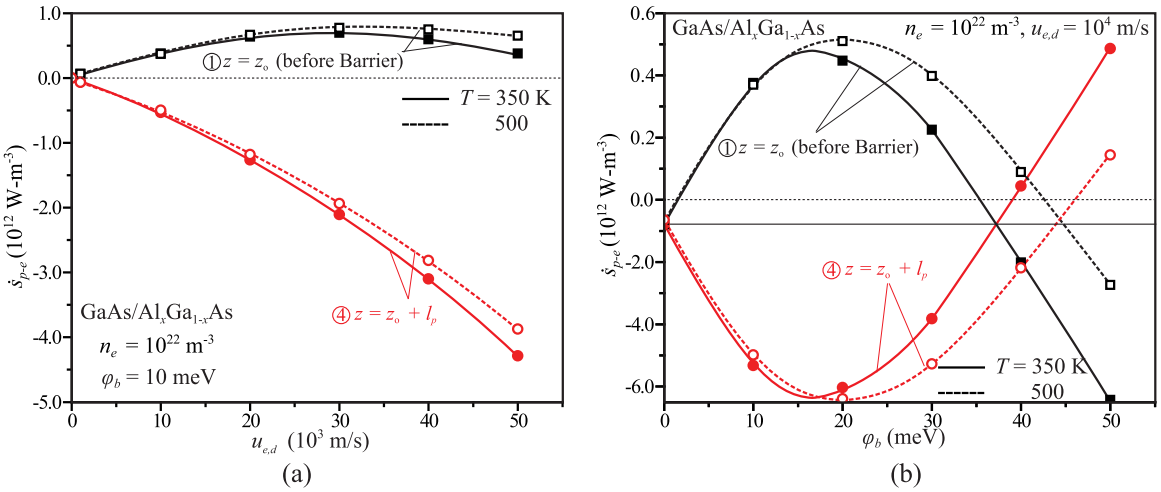

FIG. 3. (Color online) Variations of the net phonon absorption rates with respect to (a) the drift velocity and (b) the barrier height, for specified temperature (T_e = 350 and 500 K) at locations [z_o and $z_o + l_p$, in Fig. 2(c)]. A larger population of electrons is expected with larger current ($u_{e,d}$) and barrier height (φ_b). So, with the population of emission-favorable electrons (among the reflected electrons) surpassing the population of absorption-favorable electrons (under optimal $u_{e,d}$ and φ_b), the net absorption rate at location z_o decreases.

At higher temperatures, the electron distribution broadens, and this reduces its asymmetry. The larger phonon population enhances phonon absorption, with the phonon occupancy (Bose-Einstein) decreasing with phonon energy ($E_{p,O}$) and increasing with phonon temperature ($T_{p,O}$). So, high $T_{p,O}$ and low $E_{p,O}$ are desirable, hence the GaAs/AlGaAs heterobarrier system is more effective than GaN/AlGaN (which has 2.6 times larger optical phonon energy, i.e., 12 times smaller population, at 300 K [20]).

The e-p interactions across the barrier cause larger momentum change (larger effective mass, $|\hbar^2\boldsymbol{\kappa}_{e,1}^2 - \hbar^2\boldsymbol{\kappa}_{e,2}^2| = 2m_{e,e}E_{p,LO}$). The optical phonon energy also changes, but this is small compared to the $m_{e,e}$ change (e.g., 1% x_{Al} change causes 1.3% $m_{e,e}$ and 0.055% $E_{p,LO}$ changes [21]). So, through the phonon emission after the barrier transition, the electron momentum recovers with smaller electron kinetic energy loss, i.e., fewer phonons are emitted than absorbed for the momentum recovery, converting the net absorbed phonon energy to the electric potential. Thus, the barrier should be followed by a large forward field (for phonon absorption with smaller $m_{e,e}$ and emission with larger $m_{e,e}$), and this barrier height and field should be properly selected for given current and temperature.

III. MONTE CARLO SIMULATIONS, PHONON RECYCLING, AND NET POTENTIAL GAIN

The electron current channel with the phonon-recycling heterobarrier grading is simulated using the self-consistent MC method (incorporating barrier-caused electron nonequilibrium occupancy), and improving on our previous simpler analysis (with the nonconserving lateral momentum neglecting the Al-alloying effects on the transport and scattering) [5]. In the self-consistent MC method applied here, the dynamics of sampled electrons is calculated by Eq. (1), and for the barrier transition, assuming the conservation of the lateral momentum and energy, the wave vector after barrier transition and electron transmission is calculated using Eq. (3).

Electrons in the Γ, L, and X valleys are simulated, and in addition to the intravalley polar optical-phonon interactions, other interaction mechanisms including the acoustic phonon, alloy, and impurity and intervalley scatterings are included. The nonparabolic band approximation is employed for all three valleys, and the internal electric field due to the charge redistribution nonuniformity is considered with the Poisson equation [22] and updated in 5 fs time steps. Initially 100 electrons/nm are sampled, over up to 3 μm length (300 000 electrons). Electrons with equilibrium distributions from 300 to 500 K are initially prescribed and injected from the boundaries for consistent electron flow. Interaction rates for the above-mentioned mechanisms are derived from the Fermi golden rule (based on the perturbation theory), and the relations and carrier properties for these interactions are given in [3,19,21,23,24].

The drift velocity ($u_{e,d}$), particle density (n_e), and net phonon emission ($\dot{s}_{e\text{-}p}$) are ensemble-averaged over the sampled particles for the last 0.5 ns of 1.0 ns simulations. The calculated $u_{e,d}$ dependence on the electric field (e_e), e.g., the electron mobility of GaAs, $\mu_e = u_{e,d}/|e_e| = 0.84$ m^2/V s at 300 K, is in good agreement with the experiments and other simulations [25,26]. The mobility depends on the Al content through the properties affecting the scattering rates and dynamics (e.g., effective mass, dielectric constant), and Fig. 4(a) shows the x_{Al} dependence of $Al_xGa_{1-x}As$ mobility, which is approximated with $\mu_e = 0.8 - 2.2x_{Al} + x_{Al}^2$ m^2/V s suggested in [27] and reproduced by our MC simulations.

The net potential gain ($\Delta\varphi_{e,g,o}$) at the end of the barrier ($z_o + l_p$) relative to no barrier [Fig. 1(b)] is $\Delta\varphi_{e,g,o} = \Delta\varphi_{bg}(= e_c e_{e,bg} l_p) + \varphi_b - \Delta\varphi_{grad}(= e_c e_{e,grad} l_p)$. We aim at *in situ* phonon recycling subject to no electric current loss to avoid affecting the device operation upstream [i.e., the electric current density j_e (or $u_{e,d}$) is maintained under potential gain]. The electric current (given carrier density) increases with background field ($\Delta\varphi_{bg}$ for given barrier length), but it decreases with $\Delta\varphi_{e,g,o}$. For a given barrier height and length, $\Delta\varphi_{e,g,o}$ is controlled by the magnitude of $e_{e,grad}$ (or

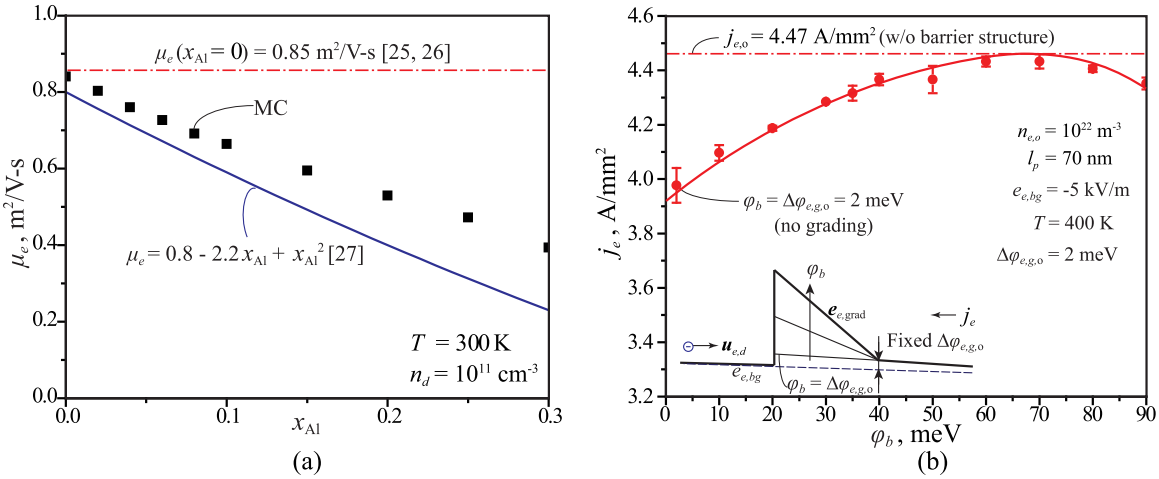

FIG. 4. (Color online) (a) Variations of electron mobility with respect to the Al content at 300 K, comparing experimental results shown with a correlation to the MC results. (b) Variations of current density with respect to barrier height, for the conditions shown and a net potential gain $\Delta\varphi_{e,g,o} = 2$ meV. The case of no grading results in current loss, and very large barrier height and grading also result in current loss.

x_{Al} grading), and there is a $\Delta\varphi_{e,g,o}$ that maintains the current density j_e (or $u_{e,d}$). Figure 4(b) shows that for $\Delta\varphi_{e,g,o} =$ 2 meV, j_e varies with the barrier height (φ_b) and grading field ($e_{e,grad}$), and the barrier structure without grading (similar to thermionic cooling) reduces j_e. This current loss is avoided in the phonon recycling through losing some of the potential gained (i.e., nonzero $e_{e,grad}$).

Due to lower mobility at larger x_{Al}, using a long barrier (l_p) and downstream lengths (l_d) results in additional resistance (current loss). The MC simulations use the scattering rate (or relaxation length) depending on the energies and mechanisms, and even those interactions within the relaxation length are included (although with small probability). Since the interaction involving high-energy electrons is more probable (mostly phonon emission), they have a short relaxation length. The phonon interaction over the barrier leads to phonon emission, but it is also required for the momentum recovery for potential gain. An optimum $l_p = 70$ nm barrier length is selected to allow the electrons to interact with phonons on the barrier, while avoiding excessive potential loss resulting from larger l_p. Under the goal of net potential gain, the downstream region will have a nonzero x_{Al}, and the larger the gain (or x_{Al}), the larger the mobility loss. So, it is desirable to locate the heterobarrier structure near the terminals in the circuit to reduce l_d. The l_d corresponding to 1 meV of potential gain (considering the difference in mobility) is larger than 5.5 μm for $|e_{e,bg}| < 50$ kV/mm, and it decreases with $|e_{e,bg}|$.

The barrier structures with no current loss are calculated, and Fig. 5 shows the variation of net potential gain $\Delta\varphi_{e,g,o}$ with respect to φ_b for several electric fields ($e_{e,bg}$). For a given field $e_{e,bg}$, the optimal barrier height $\varphi_{b,max}$ maximizing the net potential gain $\Delta\varphi_{e,g,o}$ is marked ($\Delta\varphi_{e,g,o}$ increases with φ_b up to $\varphi_{b,max}$ and then decreases). $\varphi_{b,max}$ increases as $|e_{e,bg}|$ (or current) decreases, and larger $\Delta\varphi_{e,g,o,max}$ is expected with higher $\varphi_{b,max}$. Note that using a larger optical-phonon energy material, e.g., $Al_xGa_{1-x}N$ $m_{e,e} = 0.33x_{Al} + 0.21(1 - x_{Al})$, from [28,29], the barrier system would not have a significant potential gain because of the small phonon population.

IV. SPATIAL VARIATIONS AND PHONON RECYCLING

Figures 6(a)–6(c) show the spatial distributions of the electron density n_e, average drift velocity $u_{e,d}$, electron energy E_e (kinetic + potential), potential gain $\Delta\varphi_e$, and net phonon emission $\dot{s}_{e\text{-}p}$ around the barrier. The MC results are for $\varphi_b =$ 30 meV, $e_{e,bg} = -5$ kV/m, $j_e = 5.42 \times 10^6$ A/m², and at $T =$ 350 K. In addition to the prescribed potential distribution, the internal field generated by the charge redistribution [Fig. 6(b)] creates a triangular-shape potential well behind the barrier, further modifying these distributions (e.g., n_e, $u_{e,d}$, $\dot{s}_{e\text{-}p}$). This includes increasing the accumulation of the low-energy electrons and the phonon absorption upstream of the barrier. After the barrier transition, the high-E_e electrons have larger population, and there is a net phonon emission. The local net phonon-energy flow approaches the Joule heating at about 200–300 nm up- and downstream of the barrier. With the barrier, the absorption energy flow relative to the Joule heating,

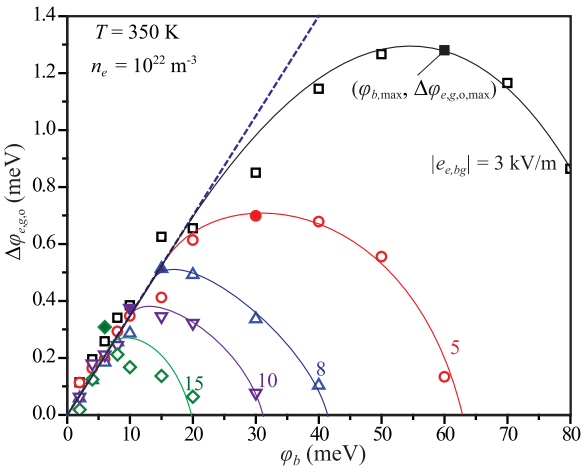

FIG. 5. (Color online) Variations of the potential gain ($\Delta\varphi_{e,g,o}$) with respect to the barrier height (φ_b), for six background field intensities ($e_{e,bg}$). An optimal potential barrier height ($\varphi_{b,max}$) exists, and this $\varphi_{b,max}$ decreases with $|e_{e,bg}|$.

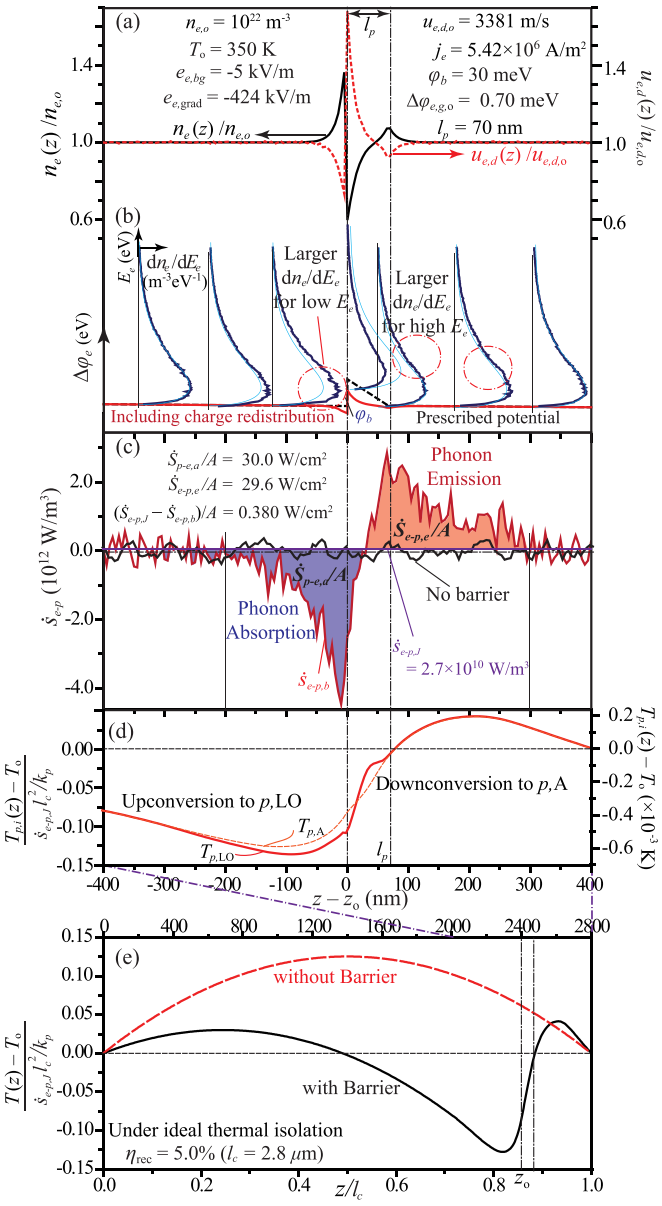

FIG. 6. (Color online) Spatial variations of (a) the electron population and velocity, (b) the electric kinetic and potential energy, (c) the net phonon emission rate, and (d) the optical and acoustic phonon temperatures near the barrier region, $[z_o - 400$ nm, $z_o + 400$ nm$]$. Since the low-energy electrons are overpopulated behind the barrier, large phonon absorption occurs there. (e) The temperature distributions with and without the barrier including the upstream region with constant Joule heating $\dot{s}_{e\text{-}p,J}$. The phonon recycling efficiency is also listed. Using the phonon emission from the MC simulations, the temperature is calculated. The recycling reduces the net phonon emission rate and the channel temperature.

$\dot{S}_{p\text{-}e,a}/A$, is larger than the emission rate, $\dot{S}_{e\text{-}p,e}/A$, so there is a net electron kinetic and potential gain from the absorption of the emitted phonons. Here, the potential net gain ($\Delta\varphi_{e,g,o}$) is only 0.7 meV, but higher potential gain is found with optimal φ_b and $e_{e,bg}$.

Under the ideal lateral thermal isolation from the surroundings, the generated phonon is preserved and no external phonon contributes to the barrier phonon-energy conversion. Using the net phonon-emission rates from the MC simulations, the temperature distribution in the channel is calculated with the finite-difference method [30].

The phonon temperature is resolved with respect to its modes, with the hot-phonon population (i.e., overpopulation) limited to the LO phonons [31]. The conservations of the LO and acoustic (A) modes are followed in each bin. The phonon energy transfer between A and LO modes is based on the three-phonon (p-p) interactions (up- and downconversion) with the associated material and phonon properties [5,8,32,33]. Using the energy conservation, the change in phonon energy (per unit area) for mode i (LO or A) in the jth bin ($z_j = z_o + j\Delta z$, bin size $\Delta z = 5$ nm) over a time step ($\Delta t, t \sim t + \Delta t$) is

$$\Delta E_{p,i}(z_j) = \Delta t\{-(q_{p,i,L} + q_{p,i,R}) + [\dot{s}_{e\text{-}p,i}(z_j) \pm \dot{s}_{p\text{-}p,\mathrm{up}}(z_j)]\Delta z\}, \quad (5)$$

where $q_{p,i,R}$ (or $q_{p,i,L}$) is the phonon flux from the neighboring bins [R: right ($j+1$), L: left ($j-1$)], $\dot{s}_{e\text{-}p,i}$ is the i-mode phonon generation rate from the e-p interactions, and $\dot{s}_{p\text{-}p,\mathrm{up}}$ is the rate of phonon upconversion to the LO mode (+ for LO and − for A).

The $q_{p,i,R}$ (or $q_{p,i,L}$) is determined from $T_{p,i}$ and $k_{p,i}$ ($k_{p,A} = 54$ W/K m and $k_{p,\mathrm{LO}} = 1$ W/K m, from [34]) as $q_{p,i,R \text{ or } L} = k_{p,i}[T_{p,i}(z_j) - T_{p,i}(z_j \pm \Delta z)]/\Delta z$. The $q_{p,i,L}$ at the left boundary is the upstream phonon generation, and the $q_{p,i,R}$ on the right is calculated using an external thermal resistance (equivalent to 20 μm of GaAs) and the surrounding temperature (T_o). The phonon temperatures are calculated using the phonon energy $E_{p,i}$ in each bin and the heat capacity $c_{p,i}$ (determined from the density of states and occupancy) [35], and these temperatures are updated for the calculation of $q_{p,i,R}$ (or $q_{p,i,L}$), $\dot{s}_{e\text{-}p,i}$, and $\dot{s}_{p\text{-}p,\mathrm{up}}$ in the next time step.

Excluding the nonequilibrium near the simulation cell boundary [9], phonon emission $\dot{s}_{e\text{-}p}$ is approximated like Fig. 1(d). With the nanometer-length barrier and much larger phonon population compared to electron population, the absolute temperature differences (including the nonequilibrium between the optical and acoustic modes) are not significant at low currents, as shown in Fig. 6(d). Then, a single phonon temperature can be used for the larger systems [including the upstream region providing phonons for the barrier transition ($\dot{s}_{e\text{-}p,\mathrm{J}}$, i.e., the Joule heating)]. The upstream length l_u is adjusted to avoid phonon flux from the end reservoirs (determined from the temperature gradient and phonon conductivity k_p). With a sufficiently large l_c, the channel can produce enough phonons for conversion in the barrier, but excessive l_c reduces the efficiency. Without the barrier, the temperature increases due to the Joule heating, and this increase depends on l_c, $\dot{s}_{e\text{-}p,\mathrm{J}}$, and k_p, so a dimensionless temperature $[T(z) - T_o]/(\dot{s}_{e\text{-}p,\mathrm{J}} l_c^2/k_p)$ is used. Figure 6(e) shows temperature distributions with and without the barrier, and it is evident that the graded barrier decreases the net phonon-emission rate.

With the electron channel connected to the two reservoirs, the phonon-recycling efficiency η_{rec} is defined as the ratio of the reduced phonon emission to the Joule heating without the

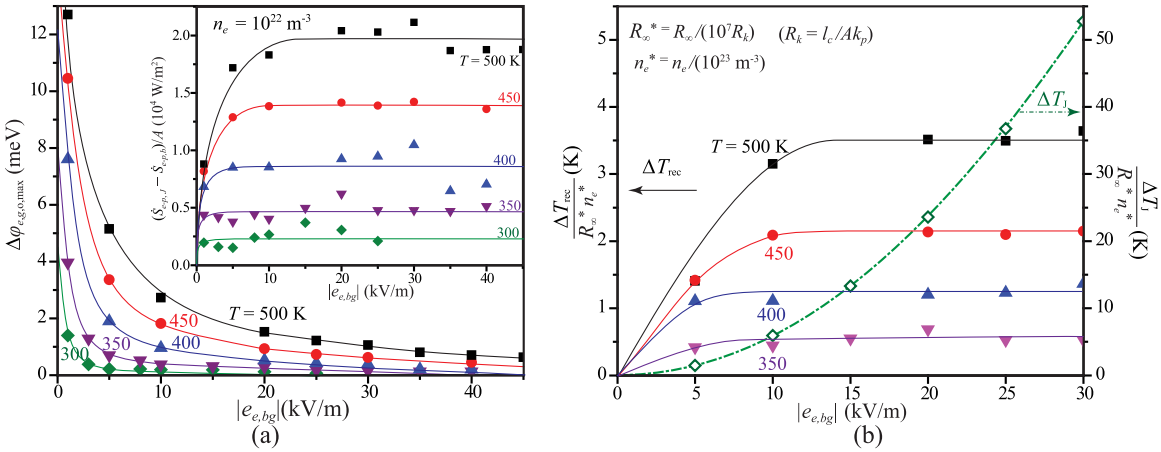

FIG. 7. (Color online) (a) Variations of the maximum potential gain ($\Delta\varphi_{e,g,o,max}$) with respect to $|e_{e,bg}|$ for five temperatures. The reduction in the phonon emission rate becomes more pronounced with an increase in temperature, as shown in the inset. (b) Variations of the temperature reduction by phonon recycling, as a function of background electric field ($e_{e,bg}$) and for four temperatures, under finite end thermal resistance R_∞. This temperature due to Joule heating without recycling is also shown to the right.

barrier, i.e.,

$$\eta_{rec} = \int_0^{l_c} (\dot{s}_{e\text{-}p,J} - \dot{s}_{e\text{-}p,b}) dz / \dot{s}_{e\text{-}p,J} l_c, \tag{6}$$

where l_c is the channel length and $\dot{s}_{e\text{-}p,b}$ is the net phonon-emission rate with the barrier structure, so η_{rec} increases with $\Delta\varphi_{e,g,o}$ for a given $e_{e,bg}$. Note that the total Joule heating is proportional to l_c, so η_{rec} also depends on l_c.

Larger $\Delta\varphi_{e,g,o,max}$ is expected as $|e_{e,bg}|$ (or current) decreases and temperature increases as in Fig. 7(a). The recycled power $[(\dot{S}_{e\text{-}p,J} - \dot{S}_{e\text{-}p,b})/A]$ in the inset of Fig. 7(a) is the product of potential gain and current density $[\Delta j_{E,e,p} = \Delta\varphi_{e,g} j_e]$, so an optimal field exists for the recycling power gain or cooling effect. Considering a steady, infinite electron channel, the Joule heating rate $\dot{s}_{e\text{-}p,J}$ $(= e_{e,bg} j_e = \mu_e e_c n_e e_{e,bg}^2)$ raises the channel temperature (ΔT_J), and this depends on the external thermal resistance between the channel and its end thermal boundaries ($R_\infty = AR_\infty/p_s l_c$, where AR_∞ is the areal thermal resistance at the two ends of the channel and p_s is the channel perimeter). This temperature rise is shown in Fig. 7(b) as a function of the field for a finite R_∞ (scaled with the internal thermal resistance R_k defined as l_c/Ak_p), whereas under an ideal end thermal isolation ($R \to \infty$), ΔT_J would tend toward infinity. The operating-temperature reduction (maximum temperature along the channel with inclusion of the barrier structure) due to the phonon recycling (ΔT_{rec}) is also shown, and as expected it increases with R_∞ and n_e. This reduction is the most significant for large background field (>10 kV/m), but the fraction of ΔT_{rec} compared to ΔT_J decreases with the field.

V. REVERSIBILITY LIMIT OF PHONON RECYCLING

Without an external phonon source, the first and second laws of thermodynamics require that the electric potential should decrease, converting to phonon energy and increasing the phonon entropy and population [6]. Since reduced phonon emission (or potential drop) is desired, less phonon entropy should be generated through the phonon recycling. Fewer electrons, due to the reduced population density over the barrier (Sec. II), participate in scattering-generated entropy, and the electrons with larger $m_{e,e}$ have larger kinetic energy, so the entropy generation in the system can be reduced. For the net phonon absorption in a section, the increase in the electron entropy should be larger than the decrease in the phonon entropy. The electron temperature, for both the upstream and downstream boundaries under equilibrium, should increase, and although the electron kinetic energy increases, its potential energy decreases. Since the phonon absorption occurs before the emission, the phonon and electron temperatures under ideal thermal isolation increase across the barrier. The conversion from the electron kinetic to potential energy can be reversible, while the phonon to electron energy conversion leads to an increase in the system entropy.

Considering the absorption of phonons emitted by the Joule heating upstream, the absorbed phonon flux q_p is $\Delta\varphi_{e,J} j_e$, where the potential drop by the Joule heating upstream $\Delta\varphi_{e,J}$ is $e_{e,bg} l_u$ (or $-u_{e,d} l_u/\mu_e$, l_u is upstream length) and j_e is $e_c n_e u_{e,d}$. Without a current loss, the entropy flux change is $\Delta j_{S,e}$, which is also the net entropy-production rate in the control volume, $u_{e,d}\Delta(S_e/V)$, where $\Delta(S_e/V)$ is the electron-entropy change per unit volume (J/K m^3). The required electron-entropy change by phonon absorption is $\Delta j_{S,e} > q_p/T_p$, and $\Delta(S_e/V) > (e_c n_e u_{e,d} l_u)/(\mu_e T_p)$. Thus, the electron-entropy generation is more pronounced with larger velocity and lower temperature, and this will result in a larger potential loss for a given phonon-absorption rate. These support the results of Fig. 7(a), i.e., the potential drop is smaller (i.e., larger potential gain) for smaller current and higher temperature. Also, the e distribution with small $u_{e,d}$ is almost symmetric, so larger φ_b is required to create a more favorable phonon-absorption condition. However, a higher barrier induces larger entropy generation through the larger absorption and emission rates across the barrier (including intervalley scattering).

Since the Joule heating increases with the current, the required upstream length increases with diminishing current, and it extends to the region not affected by the barrier. With the control volume (barrier region) excluding the upstream region,

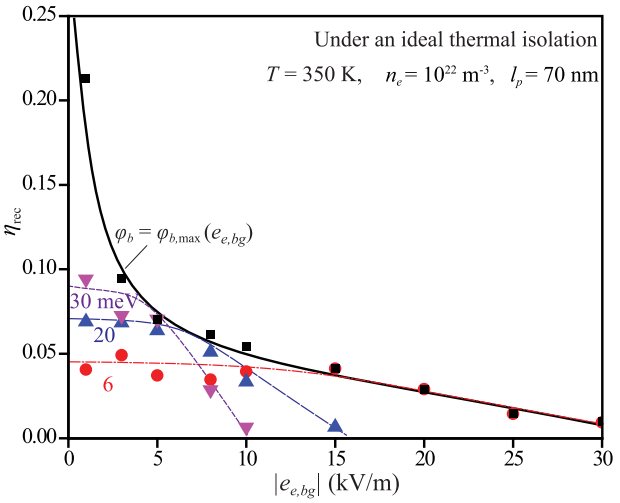

FIG. 8. (Color online) Variations of the phonon recycling efficiency with respect to $|e_{e,\mathrm{bg}}|$ for three different barrier heights (φ_b), under ideal lateral thermal isolation. The optimal barrier height ($\varphi_{b,\max}$) is also marked (with black squares).

the entropy production rate (with $T_e \simeq T_p$ at end boundaries) is

$$\Delta j_{S,e} + \Delta j_{S,p} = \left(\frac{j_{E,e,k,R} + j_{E,p,R}}{T_R} - \frac{j_{E,e,k,L} + j_{E,p,L}}{T_L} \right) > 0, \quad (7)$$

where j_i is the flux. The subscripts S and E denote entropy and energy, and L and R denote the left and right boundaries. Using the energy conservation ($\Delta j_{E,p} + \Delta j_{E,e,k} = -\Delta j_{E,e,p}$, where $\Delta j_{E,e,p}$ is the electron potential energy flux gain, i.e., the difference between $j_{E,e,p,R}$ and $j_{E,e,p,L}$), the entropy relation becomes $(T_L/T_R - 1)(j_{E,e,k,R} + j_{E,p,R}) > \Delta j_{E,e,p}$, and this sets the limit on $\Delta j_{E,e,p}$. Note that $\Delta j_{E,e,p}$ is negative (limits the reduced phonon emission) due to a temperature increase across the barrier, and the additional upstream Joule heating loss further limits η_{rec}, i.e., the phonon recycling efficiency for diminishing current should be less than the reversible limit.

For phonon recycling, under an appropriate channel length and ideal lateral thermal isolation, the predicted maximum η_{rec} is shown in Fig. 8, and it decreases with $|e_{e,\mathrm{bg}}|$. As discussed above, for higher efficiency, smaller φ_b is needed for large $|e_{e,\mathrm{bg}}|$. With diminishing current, the results show notably high η_{rec}, i.e., at 350 K, it reaches 25% of the reversible limit (η_{rec} for 1 kV/m reaches 27% at 400 K and 36% at 500 K). The required l_c for large $\Delta\varphi_{e,g,\mathrm{o}}$ increases with larger φ_b and smaller $|e_{e,\mathrm{bg}}|$, and these large l_c and φ_b limit the efficiency.

Note that the curves in Fig. 8 are drawn to fit the results, and due to the uncertainties in the MC treatments, smaller fields cannot be simulated. With vanishing fields, the Joule heating can be partially reversed by the phonon-absorbing heterobarrier. A finite lateral thermal isolation causes smaller η_{rec}, due to the phonon leakage, and this reduction is more pronounced for the larger channel lengths (small $|e_{e,\mathrm{bg}}|$). In the constant potential power gain $\Delta j_{E,e,p}$ regime occurring for high $|e_{e,\mathrm{bg}}|$, shown in the inset of Fig. 7(a), η_{rec} becomes $\Delta j_{E,e,p}/|e_{e,\mathrm{bg}}| j_e l_c$. Then for $\eta_{\mathrm{rec}} \geqslant 1\%$, we have $|e_{e,\mathrm{bg}}| \leqslant (\Delta j_{E,e,p}/0.01\mu_e n_e e_c l_c)^{1/2}$, e.g., the condition of $|e_{e,\mathrm{bg}}| \leqslant 30$ kV/m for 350 K and $l_c = 500$ nm.

For the enhanced phonon recycling under higher fields (larger Joule heating), the potential gain by the barrier should increase, and this can be achieved by higher barrier transmission and smaller momentum loss at the barrier. If scattering at the barrier redirects the electrons, the lateral momentum can then contribute to the transmission and translational momentum. Thus, higher recycling efficiency can be expected by controlling the barrier interface roughness and relaxing the conservation of lateral momentum [12,36].

VI. CONCLUSION

Joule heating converting electron potential energy to phonon energy is partially reversed by harvesting the emitted phonons for electron transition across a potential barrier. For the recovery of the momentum loss by this barrier transition, a potential grading formed by alloying should follow the barrier, and this barrier-grading structure is designed for the smallest potential loss for effective phonon recycling.

In the 1D electron transport, momentum lateral to the transport direction is invariant with the potential distribution without electron scatterings, and this lateral momentum conservation is utilized in the electron dynamics under the potential distribution. The momentum decrease of the transmitted electrons in the transport direction and the barrier reflection are more significant compared to the previously studied nonconserving lateral momentum. However, they are alleviated by the effective-mass increase across the barrier (due to alloying), which also improves the momentum relaxation and electron kinetic energy gain on the graded barrier. The structure optimized here reduces the overall entropy generation and the net phonon emission, under small current and high phonon population. With vanishing current, the entropy generation rate is further reduced with large barrier heights, thus increasing the recycling efficiency.

Since the lateral momentum contributes to the transmission, higher recycling efficiency is expected by including partially nonconserving lateral momentum electron scattering at the barrier. A large phonon source upstream (increase in phonon population) and a heterostructure composition with a large effective-mass variation [for maintaining adequate phonon energy ($\sim k_B T$)] further improve the barrier energy conversion. *In situ* phonon recycling (without an external device) improves the energy conversion efficiency (reduces the electric potential loss) and transport in the related circuits, and it reduces thermal management load, enhancing the performance of transistors, diodes (e.g., LED), solar cells, etc.

ACKNOWLEDGMENTS

This work was supported by the NSF Program on Thermal Transport and Processes (Award No. CBET 1332807) and the DOE Center for Solar and Thermal Energy Conversion at the University of Michigan (Office of Basic Energy Sciences, Award No. DE-SC0000957) and computing resources of DOE National Energy Research Scientific Computing (Office of Science, Contract No. DE-AC02-05CH11231). This research

used resources of the National Energy Research Scientific Computing Center, a DOE Office of Science User Facility supported by the Office of Science of the U.S. Department of Energy under Contract No. DE-AC02-05CH11231.

[1] C. E. Mungan, Thermodynamics of radiation-balanced lasing, J. Opt. Soc. Am. B **20**, 1075 (2003).
[2] S. R. Bowman, S. P. O'Connor, S. Biswal, N. J. Condon, and A. Rosenberg, Minimizing heat generation in solid-state lasers, IEEE J. Quantum Electron. **46**, 1076 (2010).
[3] M. Lundstrom, *Fundamentals of Carrier Transport* (Cambridge University Press, Cambridge, 2000).
[4] M. Kaviany, *Heat Transfer Physics*, 2nd ed. (Cambridge University Press, Cambridge, 2014).
[5] S. Shin, C. Melnick, and M. Kaviany, Heterobarrier for converting hot-phonon energy to electric potential, Phys. Rev. B **87**, 075317 (2013).
[6] S. Shin and M. Kaviany, Entropy production in hot-phonon energy conversion to electric potential, J. Appl. Phys. **114**, 083710 (2013).
[7] A. Matulionis, J. Liberis, I. Matulionien, H. Y. Cha, L. F. Eastman, and M. G. Spencer, Hot-phonon temperature and lifetime in biased 4H-SiC, J. Appl. Phys. **96**, 6439 (2004).
[8] G. P. Srivastava, *The Physics of Phonons* (Hilger, Bristol, 1990).
[9] M. Zebarjadi, A. Shakouri, and K. Esfarjani, Thermoelectric transport perpendicular to thin-film heterostructures calculated using the Monte Carlo technique, Phys. Rev. B **74**, 195331 (2006).
[10] C. M. Wu and E. S. Yang, Carrier transport across heterojunction interfaces, Solid-State Electron. **22**, 241 (1979).
[11] R. Kim, C. Jeong, and M. Lundstrom, On momentum conservation and thermionic emission cooling, J. Appl. Phys. **107**, 054502 (2010).
[12] D. Vashaee and A. Shakouri, Improved thermoelectric power factor in metal-based superlattices, Phys. Rev. Lett. **92**, 106103 (2004).
[13] B. Huard, J. A. Sulpizio, N. Stander, K. Todd, B. Yang, and D. Goldhaber-Gordon, Transport measurements across a tunable potential barrier in graphene, Phys. Rev. Lett. **98**, 236803 (2007).
[14] R. Cobbold, *Theory and Applications of Field-effect Transistors* (Wiley-Interscience, New York, 1970).
[15] K. Yang, J. R. East, and G. I. Haddad, Numerical modeling of abrupt heterojunctions using a thermionic-field emission boundary condition, Solid-State Electron. **36**, 321 (1993).
[16] K. Horio and H. Yanai, Numerical modeling of heterojunctions including the thermionic emission mechanism at the heterojunction interface, IEEE Trans. Electron Devices **37**, 1093 (1990).
[17] Q. S. Zhu, S. M. Mou, X. C. Zhou, and Z. T. Zhong, Determination of the conduction-band offset of a single AlGaAs barrier layer using deep level transient spectroscopy, Appl. Phys. Lett. **62**, 2813 (1993).
[18] M. E. Levinshtein, S. L. Rumyantsev, and M. Shur, *Handbook Series on Semiconductor Parameters* (World Scientific, London, 1996).
[19] M. A. R. Al-Mudares and B. K. Ridley, Monte Carlo simulation of scattering-induced negative differential resistance in AlGaAs/GaAs quantum wells, J. Phys. C **19**, 3179 (1986).
[20] M. E. Levinshtein, S. L. Rumyantsev, and M. S. Shur, *Properties of Advanced Semiconductor Materials GaN, AlN, InN, BN, SiC, SiGe* (Wiley-Interscience, New York, 2001).
[21] S. Adachi, GaAs, AlAs, and $Al_xGa_{1-x}As$: Material parameters for use in research and device applications, J. Appl. Phys. **58**, R1 (1985).
[22] C. Moglestue, *Monte Carlo Simulation for Semiconductor Device* (Chapman and Hall, London, UK, 1993).
[23] T. R. Parker, C. C. Phillips, and P. G. May, $Al_xGa_{1-x}As$ intervalley scattering rates from field-assisted photoemission spectroscopy, Phys. Rev. B **51**, 4264 (1995).
[24] A. Dargys and J. Kundrotas, *Handbook on Physical Properties of Ge, Si, GaAs and InP* (Science and Encyclopedia Publishers, Vilnius, 1994).
[25] J. Ruch and G. Kino, Transport Properties of GaAs, Phys. Rev. **174**, 921 (1968).
[26] P. Houston and A. Evans, Electron drift velocity in n-GaAs at high electric fields, Solid State Electron. **20**, 197 (1977).
[27] J. S. Blakemore, Semiconducting and other major properties of gallium arsenide, J. Appl. Phys. **53**, R123 (1982).
[28] J. Piprek, *Nitride Semiconductor Devices: Principles and Simulation* (Wiley-VCH, Weinheim, 2007).
[29] K.-S. Lee, D.-H. Yoon, S.-B. Bae, M.-R. Park, and G.-H. Kim, Self-Consistent Subband calculations of AlGaN/GaN Single Heterojunctions, ETRI J. **24**, 270 (2002).
[30] M. Kaviany, *Essentials of Heat Transfer* (Cambridge University Press, Cambridge, 2011).
[31] K. Kim, K. Hess, and F. Capasso, Monte Carlo study of electron heating and enhanced thermionic emission by hot phonons in heterolayers, Appl. Phys. Lett. **52**, 1167 (1988).
[32] W. Cai, M. C. Marchetti, and M. Lax, Nonequilibrium phonon effect on time-dependent relaxation of hot electrons in semiconductor heterojunctions, Phys. Rev. B **35**, 1369 (1987).
[33] V. Spagnolo, G. Scamarcio, M. Troccoli, F. Capasso, C. Gmachl, A. M. Sergent, A. L. Hutchinson, D. L. Sivco, and A. Y. Cho, Nonequilibrium optical phonon generation by steady-state electron transport in quantum-cascade lasers, Appl. Phys. Lett. **80**, 4303 (2002).
[34] T. Luo, J. Garg, J. Shiomi, K. Esfarjani, and G. Chen, Gallium arsenide thermal conductivity and optical phonon relaxation times from first-principles calculations, Europhys. Lett. **101**, 16001 (2013).
[35] S. Tiwari, *Compound Semiconductor Device Physics* (Academic, San Diego, 1992).
[36] Z. Bian and A. Shakouri, Enhanced solid-state thermionic emission in nonplanar heterostructures, Appl. Phys. Lett. **88**, 012102 (2006).